Inverse correlation between fatty acid transport protein 4 and vision in Leber congenital amaurosis associated with RPE65 mutation

Songhua Li[a], William C. Gordon[a], Nicolas G. Bazan[a], and Minghao Jin[a,1]

[a]Neuroscience Center of Excellence, School of Medicine, Louisiana State University Health Sciences Center, New Orleans, LA 70112

Edited by Steven J. Fliesler, University at Buffalo, State University of New York, Buffalo, NY, and accepted by Editorial Board Member Jeremy Nathans October 12, 2020 (received for review June 22, 2020)

Fatty acid transport protein 4 (FATP4), a transmembrane protein in the endoplasmic reticulum (ER), is a recently identified negative regulator of the ER-associated retinal pigment epithelium (RPE)65 isomerase necessary for recycling 11-*cis*-retinal, the light-sensitive chromophore of both rod and cone opsin visual pigments. The role of FATP4 in the disease progression of retinal dystrophies associated with RPE65 mutations is completely unknown. Here we show that FATP4-deficiency in the RPE results in 2.8-fold and 1.7-fold increase of 11-*cis*- and 9-*cis*-retinals, respectively, improving dark-adaptation rates as well as survival and function of rods in the Rpe65 R91W knockin (KI) mouse model of Leber congenital amaurosis (LCA). Degradation of S-opsin in the proteasomes, but not in the lysosomes, was remarkably reduced in the KI mouse retinas lacking FATP4. FATP4-deficiency also significantly rescued S-opsin trafficking and M-opsin solubility in the KI retinas. The number of S-cones in the inferior retinas of 4- or 6-mo-old KI;*Fatp4*$^{-/-}$ mice was 7.6- or 13.5-fold greater than those in age-matched KI mice. Degeneration rates of S- and M-cones are negatively correlated with expression levels of FATP4 in the RPE of the KI, KI;*Fatp4*$^{+/-}$, and KI;*Fatp4*$^{-/-}$ mice. Moreover, the visual function of S- and M-cones is markedly preserved in the KI;*Fatp4*$^{-/-}$ mice, displaying an inverse correlation with the FATP4 expression levels in the RPE of the three mutant lines. These findings establish FATP4 as a promising therapeutic target to improve the visual cycle, as well as survival and function of cones and rods in patients with RPE65 mutations.

RPE65 | visual cycle | opsin solubility | cone photoreceptor | retinal degeneration

Retinal pigment epithelium 65 (RPE65) is a key retinoid isomerase (1–4) in the visual cycle responsible for recycling 11-*cis*-retinal (11*c*RAL), which functions not only as a molecular switch for initiating the phototransduction in response to light stimuli, but also as a chaperone for normal trafficking of cone opsins to the outer segments (OS) of cones (5, 6). RPE65 is also the isomerase responsible for the production of *meso*-zeaxanthin (7), one of the three macular pigments in the human retina that function as potent antioxidants and light-screening pigments to protect the macula (8). Expression levels and activities of RPE65 are positively correlated with an increase in both retinal susceptibility to light-induced degeneration (9, 10) and the accumulation rates of the visual cycle-derived cytotoxic bisretinoids, the major autofluorescent components of lipofuscin implicated in Stargardt disease and geographic atrophy of age-related macular degeneration (11–13).

Mutations in the *RPE65* gene cause vision impairment and retinal degeneration in affected patients, canines, and mice. In humans, more than 100 DNA variants in the *RPE65* gene are reported as pathogenic mutations causing retinal degenerative diseases (Global Variome shared LOVD: https://databases.lovd.nl/shared/genes/RPE65). Although night blindness is the first significant symptom in most patients with RPE65 mutations, in vivo microscopy of the fovea demonstrated that many patients exhibited severe cone degeneration at very early ages (14, 15). The potentially important role of RPE65 in maintaining human cone photoreceptor health and vision is also supported by its abundant expression and higher activity in the macaque central RPE layer localized to the cone-rich area (16).

With the exception of adeno-associated virus (AAV)-based gene therapy, there is no approved effective treatment available for diseases caused by RPE65 mutations. In clinical trials, subretinaly injected AAV-RPE65 has improved vision in some patients (17–20). However, subsequent studies showed that the gene therapy could not stop progressive retinal degeneration in patients (21–23). In addition, more than half of the subjects injected with a higher dose of AAV-RPE65 developed various degrees of intraocular inflammation (23). AAV *cis*-regulatory sequences are associated with toxic effects on the RPE and microglial cells (24). Lower dose of AAV-RPE65 may reduce the side effects but it will limit the beneficial outcome of this very high-cost therapy because only a small population of RPE cells will express the exogenous RPE65 (17). These studies suggest the need for alternative interventions and improved gene therapy to prevent progressive retinal degeneration in patients.

A recent study showed that systemic administration of 4-phenylbutyrate (PBA) could partially rescue the function of mutated RPE65, thereby improving the preservation of photoreceptors and vision in a mouse model of Leber congenital amaurosis

Significance

Mutations in the retinal pigment epithelium (RPE)65 are associated with Leber congenital amaurosis (LCA), for which there is no effective therapy alleviating progressive retinal degeneration in affected patients. Here, we show that fatty acid transport protein 4 (FATP4)-deficiency markedly increases synthesis of 11-*cis*- and 9-*cis*-retinals, improving solubility, stability, and trafficking of cone opsins in the R91W knockin (KI) mouse model of LCA. Numbers of S-cones in 6-mo-old KI;Fatp4-/- mouse retinas were 13.5-fold greater than those in age-matched KI mice. Survival and function of S- and M-cones are negatively correlated with expression levels of FATP4 in the RPE of KI, KI;Fatp4+/-, and KI;Fatp4-/- mice. These findings establish FATP4 as a promising therapeutic target to preserve vision in patients with RPE65 mutations.

Author contributions: S.L. and M.J. designed research; S.L. and M.J. performed research; W.C.G. and N.G.B. contributed new reagents/analytic tools; S.L., W.C.G., N.G.B., and M.J. analyzed data; and S.L. and M.J. wrote the paper.

The authors declare no competing interest.

This article is a PNAS Direct Submission. S.J.F. is a guest editor invited by the Editorial Board.

[1]To whom correspondence may be addressed. Email: mjin@lsuhsc.edu.

This article contains supporting information online at https://www.pnas.org/lookup/suppl/doi:10.1073/pnas.2012623117/-/DCSupplemental.

First published November 30, 2020.

(LCA) (25). This study suggests that rescuing the intrinsic function of mutated RPE65 has the potential to mitigate retinal degeneration in patients with RPE65 mutations. Studies in cultured cells have shown that many RPE65 mutants could be rescued by chemical and physical treatments (26, 27). These studies have provided the basis to explore new therapeutic strategies for diseases associated with RPE65 mutations. One of the possible approaches that can rescue RPE65 mutants, and thereby enhance the efficacy of the gene therapy and PBA-treatment, is to modulate endogenous regulators of RPE65.

Through screening of RPE cDNA libraries, we have previously identified fatty acid transport protein 4 (FATP4) as a negative regulator of RPE65 (28). FATP4 is a transmembrane protein with an endoplasmic reticulum (ER)-localization domain (29). Among the six members of the FATP family, FATP4 is the most abundant FATP in the RPE. It has fatty acyl-CoA synthetase activity with specificity toward saturated and monounsaturated very long-chain fatty acids. Activation of C24:0, but not C16:0, fatty acid was reduced in the FATP4-null mouse cells (30, 31). In an in vitro assay for RPE65 isomerase, lignoceroyl (C24:0)-CoA inhibited the synthesis of 11-*cis*-retinol (11*c*ROL), whereas palmitoyl (C16:0)-CoA promoted the synthesis of 11*c*ROL (28). In addition, FATP4 has been shown to interact with RPE65 and inhibits 11*c*ROL synthesis catalyzed by RPE65 (32). Consistent with these studies, the retinoid isomerase activity and the visual cycle rates are increased in a mouse line lacking FATP4 in the RPE (28).

In the present study, we investigated the role and mechanisms of FATP4 function in regulating the visual cycle, as well as survival and function of rod and cone photoreceptors in pathological conditions caused by hypomorphic R91W RPE65, the most common RPE65 mutant linked to LCA. The R91W mutation has been shown to cause early degeneration of cones in affected patients and animal models (33, 34). We found that FATP4 is a promising therapeutic target to preserve cones and vision in patients with RPE65 mutation.

Results

Deletion of FATP4 Increased Synthesis of 11cRAL and 9-*cis*-Retinal in the R91W Knockin Mouse Model of LCA. To investigate the role of

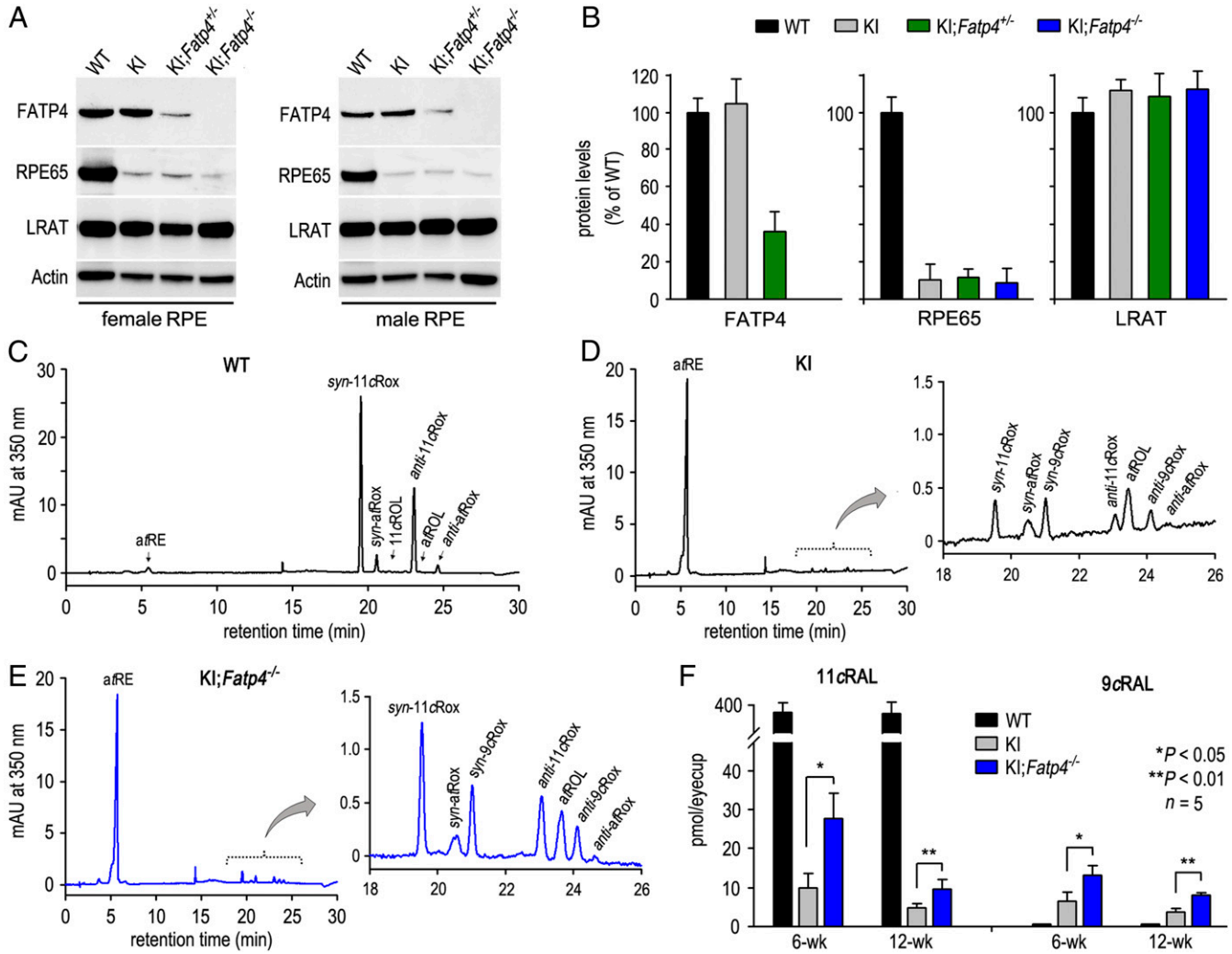

Fig. 1. Deletion of FATP4 increased chromophore synthesis in R91W KI mice. (*A*) Immunoblot analysis of FATP4, RPE65, and LRAT in the mouse RPE with the indicated genotypes. β-Actin was detected as a loading control. (*B*) Relative expression levels of FATP4, RPE65, and LRAT in the mutant mouse RPE were normalized by actin levels and shown as percent of each protein level in WT mice. (*C–E*) Representative HPLC chromatograms of ocular retinoids extracted from dark-adapted WT (*C*), KI (*D*), and KI;*Fatp4*$^{-/-}$ (*E*) mice. The marked peaks are *at*RE, *syn*-11-*cis* retinal oxime (*syn*-11cRox), *syn*-all-*trans* retinal oxime (*syn*-atRox), 11cROL, anti-11-*cis* retinal oxime (*anti*-11cRox), all-*trans* retinol (atROL), anti-all-*trans* retinal oxime (*anti*-atRox), *syn*-9-*cis* retinal oxime (*syn*-9cRox), and anti-9-*cis* retinal oxime (*anti*-9cRox). (*F*) Amounts of 11-*cis* and 9-*cis* retinals in dark-adapted eyes of 6-wk- and 12-wk-old WT, KI, and KI;*Fatp4*$^{-/-}$ mice are measured by HPLC analysis.

FATP4 in disease progress of the knockin (KI) mouse, we generated KI mouse lines with a *Fatp4*$^{-/-}$ or *Fatp4*$^{+/-}$ genotype. Immunoblot analysis of RPE showed that RPE65 expression levels in KI, KI;*Fatp4*$^{+/-}$, and KI;*Fatp4*$^{-/-}$ mice were ~10% of WT RPE65 (Fig. 1 *A* and *B*). This observation is consistent with the previous study showing rapid degradation of R91W RPE65 through the ubiquitin-proteasomal pathway (25) and suggests that FATP4 had no significant effect on the stability of the mutant RPE65. Expression levels of lecithin:retinol acyltransferase (LRAT), which synthesizes the substrate of RPE65, in all mutant lines were similar to that in the WT mouse RPE. FATP4 expression was reduced by 60% in the KI;*Fatp4*$^{+/-}$ RPE, as compared to the WT mouse RPE, and was not detectable in the KI;*Fatp4*$^{-/-}$ mouse RPE (Fig. 1 *A* and *B*).

We then analyzed ocular retinoids in the mice. To stabilize the highly reactive retinals, we converted 11*c*RAL and all-*trans*-retinal into syn- and antiretinaloxime isomers using hydroxylamine (35). HPLCy (HPLC) data showed that the amounts of 11*c*RAL and 9-*cis*-retinal (9*c*RAL), a functional iso-chromophore (36), were increased 2.8-fold and 1.7-fold, respectively, in the dark-adapted KI;*Fatp4*$^{-/-}$ mice (Fig. 1*F*), whereas the amounts of all-*trans*-retinal, all-*trans*-retinol, and all-*trans*-retinyl esters in the KI;*Fatp4*$^{-/-}$ mice were not significantly changed, as compared to those in age-matched KI mice (Fig. 1 *C–F* and *SI Appendix*, Table S1).

FATP4-Deficiency Accelerated Recovery of Rod Light Sensitivity and 11cRAL Synthesis in the KI Mice. To know whether the increased 11*c*RAL in the KI;*Fatp4*$^{-/-}$ mice (Fig. 1) is associated with an improvement of the visual cycle, we compared recovery rates of rod light sensitivities in KI and KI;*Fatp4*$^{-/-}$mice. After photobleaching rhodopsin, we put mice in the dark for different times. We then recorded scotopic electroretinograms (ERG) of the mice. KI and KI;*Fatp4*$^{-/-}$ mice kept in darkness for 15 min exhibited similar amplitudes of *a*-waves in response to a series of light flashes (50~250 cd·s/m^2). However, *a*-wave amplitudes of KI;*Fatp4*$^{-/-}$ mice dark-adapted for 30 min or 45 min were significantly greater than those of the KI mice under the same light conditions (Fig. 2 *A* and *B*). To confirm these results, we measured recovery of 11*c*RAL synthesis in the mice adapted to dark for different times. Since KI and KI;*Fatp4*$^{-/-}$ mice contain small amounts of the visual chromophores, we kept mice in darkness for 1 or 2 h after photobleaching the visual pigments. As shown in Fig. 2*C*, the amounts of 11*c*RAL in KI;*Fatp4*$^{-/-}$ mice kept in darkness for 1 and 2 h were significantly greater than those in KI mice at the same dark-adaptation conditions.

Alleviation of Rod Degeneration in the KI Mice Lacking FATP4. The KI mice exhibit a disorganization of photoreceptor OS as early as 4 wk of age, and this OS disorganization/degeneration advances with aging (37). To know whether FATP4-deficiency attenuates rod degeneration in KI mice, we performed immunocytochemistry of rhodopsin in WT, KI, and KI;*Fatp4*$^{-/-}$ mice. As shown in Fig. 3 *A–C*, the lengths of rod OS in 4- and 6-mo-old KI;*Fatp4*$^{-/-}$ mice are much longer than those in age-matched KI mice. The thickness of the outer nuclear layer (ONL) was also preserved in 6-mo-old KI;*Fatp4*$^{-/-}$ mice as compared to that of 6-mo-old KI mice (Fig. 3*C*). Consistent with these observations, quantitative immunoblot analysis showed that expression levels of rhodopsin were increased by ~40% or ~70%, respectively, in 2- or 4-mo-old KI;*Fatp4*$^{-/-}$ mice, as compared to age-matched KI mice (Fig. 3 *D* and *E*), while expression levels of rhodopsin in 2- and 4-mo-old KI mice were ~50% or 40% of those in age-matched WT mice (Fig. 3 *D* and *E*).

Improved Trafficking, Stability, and Solubility of Cone Opsins in KI;*Fatp4*$^{-/-}$ Mice. Lack and severe shortage of 11*c*RAL supply due to RPE65 mutations cause cone opsin mislocalization in animal models (5, 6, 34). Since 11*c*RAL and 9*c*RAL are increased in the KI;*Fatp4*$^{-/-}$ mice, we tested whether S-opsin mislocalization is reduced in the KI;*Fatp4*$^{-/-}$ retina. Immunohistochemistry of S-opsin showed that mislocalization of S-opsin was significantly reduced in the KI;*Fatp4*$^{-/-}$ retinas as compared to the KI retinas (Fig. 4*A*). Quantitative analysis revealed that S-opsin mislocalization was reduced by ~40% in the KI;*Fatp4*$^{-/-}$ mice (Fig. 4*B*).

As the first step to analyze the mechanisms resulting in reduction of S-opsin mislocalization in the KI;*Fatp4*$^{-/-}$ cones, we incubated WT and mutant retinas with MG132 (a proteasome inhibitor) or pepstatin A (a lysosome inhibitor) in media of the retinal explants. Immunoblot analysis showed that the amounts of S-opsin in the KI and KI;*Fatp4*$^{-/-}$ retinas, but not in the WT retinas, were significantly increased by the treatments (Fig. 4 *C* and *D*). The relative amounts of S-opsin were increased 3-fold or 1.6-fold, respectively, in the KI and KI;*Fatp4*$^{-/-}$ retinas treated with MG132, as compared to the same genotype retinas treated with DMSO, while the relative amounts of S-opsin in the KI and KI;*Fatp4*$^{-/-}$ retinas treated with pepstatin A were increased by ~55% or ~43%, respectively, as compared to DMSO-treated retinas (Fig. 4 *C* and *D*). These results suggest that a large fraction of S-opsin proteins in the KI cones are misfolded and underwent degradation in the proteasomes. Increase in the synthesis of 11*c*RAL and 9*c*RAL in KI;*Fatp4*$^{-/-}$ mice significantly reduced the proteasomal degradation of S-opsin in the cones. The results also suggest that a small portion of S-opsin proteins in both KI and KI;*Fatp4*$^{-/-}$ retinas underwent lysosomal degradation, which could not be reduced by the increased 11*c*RAL and 9*c*RAL in the KI;*Fatp4*$^{-/-}$ retina.

To further confirm whether cone opsins are misfolded in the KI cones, we analyzed solubility of M-opsin. We homogenized retinas in PBS containing Triton X-100 detergent and separated opsins into soluble and insoluble fractions by ultracentrifugation. Immunoblot analysis of these fractions showed that more than 90% of M-opsin in the WT retina was included in the soluble fraction, whereas only ~58% of M-opsin in the KI retina was distributed to the soluble fraction (Fig. 4 *E* and *F*). In the KI;*Fatp4*$^{-/-}$ retina, the soluble M-opsin was increased to ~78% (Fig. 4 *E* and *F*). Consistent with this result, insoluble M-opsin was significantly reduced in the KI;*Fatp4*$^{-/-}$ retina, as compared to the KI retina (Fig. 4 *E* and *F*).

FATP4 Expression Levels in the RPE Are Negatively Correlated with Degeneration Rates of S- and M-Cones in the LCA Mice. In the mouse eyes, M-cones are present in the superior half of the retina while the majority of S-cones are present in the inferior half of the retina (38). To increase the detection sensitivity of cone opsins and to accurately assess the degeneration rates of S- and M-cones in the KI and KI;*Fatp4*$^{-/-}$ mice, we performed quantitative immunoblot analysis using inferior and superior halves of the mouse retinas. Approximately 85% of S-opsin (S-cones) and 92% of M-opsin (M-cones) are present in the inferior or superior half of 2-mo-old WT mouse retinas, respectively (Fig. 5 *A–C*). Expression levels of S-opsin in the inferior retinas of 2-mo-old KI;*Fatp4*$^{+/-}$ and KI;*Fatp4*$^{-/-}$ mice were 2.7-fold or 5-fold higher than that in the inferior retina of age-matched KI mice, respectively (Fig. 5 *D* and *E*). The differences of S-opsin expression levels in the KI mice and KI mice with *Fatp4*$^{+/-}$ or *Fatp4*$^{-/-}$ genotypes were enlarged to ~6-fold and 11-fold, respectively, at 4-mo-old mouse age (Fig. 5 *F* and *G*). We failed to observe a significant increase of S-opsin in the superior retinas of KI;*Fatp4*$^{+/-}$ and KI;*Fatp4*$^{-/-}$ mice (Fig. 5 *D* and *E*), possibly due to almost complete loss of S-cones in the superior retinas that contain a small population of S-cones (Fig. 5 *A–E*). On the other hand, immunoblot analysis showed a significant increase of M-opsin in the superior retinas of KI;*Fatp4*$^{+/-}$ and KI;*Fatp4*$^{-/-}$

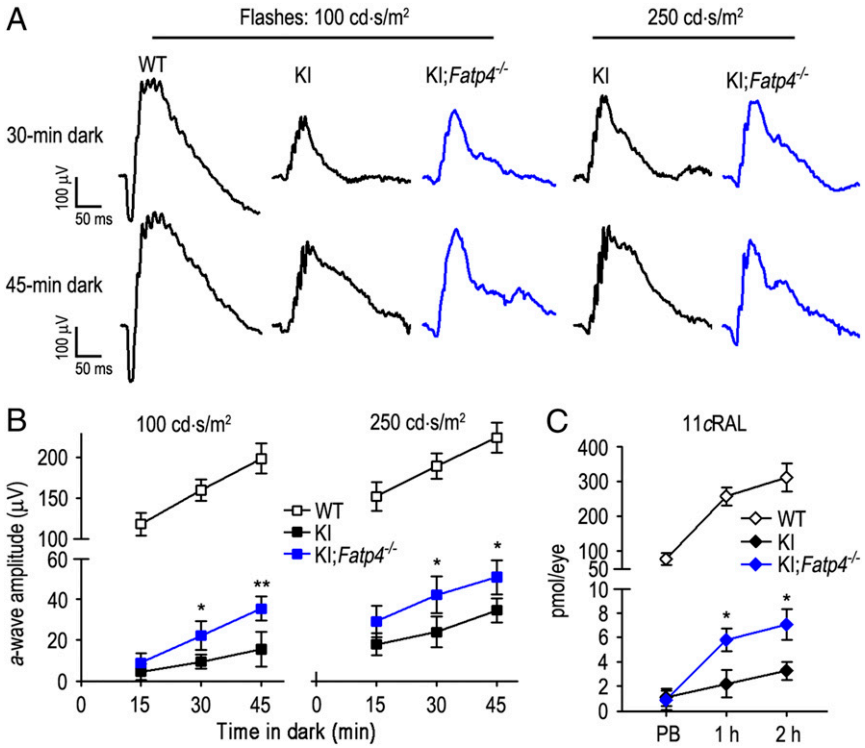

Fig. 2. Accelerated recovery of rod light sensitivity and chromophore synthesis in KI;*Fatp4*$^{-/-}$mice. (*A*) Representative scotopic ERG responses of WT, KI, and KI;*Fatp4*$^{-/-}$ mice to 100- or 250-cd·s/m^2 flashes. The mice were kept in darkness for 30 min or 45 min after photobleaching the visual pigments. (*B*) Amplitudes of scotopic ERG *a*-waves evoked by 100-cd·s/m^2 or 250-cd·s/m^2 flashes in WT, KI, and KI;*Fatp4*$^{-/-}$ mice kept in darkness for the indicated times after photobleaching the visual pigments. (*C*) Amounts of 11cRAL in WT, KI, and KI;*Fatp4*$^{-/-}$ mouse eyes are measured at the indicated conditions: Immediately after photobleaching (PB), dark-adapted for 1 h or 2 h after photobleaching. Asterisks indicate significant differences between KI and KI;*Fatp4*$^{-/-}$ mice (*$P < 0.04$, **$P \leq 0.005$). Error bars show SD ($n = 4 \sim 6$).

mice, as compared to age-matched KI mouse superior retinas (Fig. 6 *A–D*).

To confirm the results of immunoblot analysis, we performed immunohistochemistry for S- and M-opsins. The number of S-cones preserved in the inferior retinas of 4-mo-old KI;*Fatp4*$^{+/-}$ and KI;*Fatp4*$^{-/-}$ mice was 3.1-fold or 7.6-fold greater than those in age-matched KI mouse inferior retinas (Fig. 5 *H* and *I*). The number of M-opsin cells in the superior retinas of 4-mo-old KI;*Fatp4*$^{+/-}$ and KI;*Fatp4*$^{-/-}$ mice was also significantly greater than those in the superior retinas of KI mice (Fig. 6*E*).

All of the three mutant lines (KI, KI;*Fatp4*$^{+/-}$, and KI;*Fatp4*$^{-/-}$) displayed a progressive degeneration of S-cones with aging. In the KI mice, however, the degeneration rates of S-cones were much faster than those in KI;*Fatp4*$^{+/-}$ and KI;*Fatp4*$^{-/-}$.

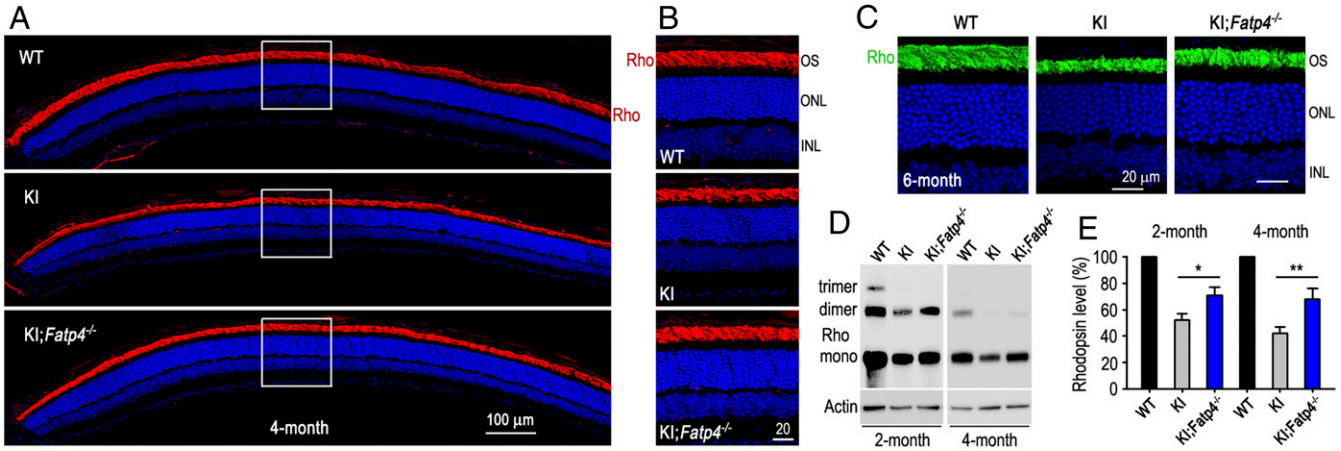

Fig. 3. FATP4-deficiency mitigated degeneration of rods in KI mice. (*A*) Immunostaining of rhodopsin (Rho, red) in the superior retinas of 4-mo-old WT, KI, and KI;*Fatp4*$^{-/-}$ mice. Nuclei were counterstained with DAPI (blue). (*B*) Higher-magnification images of the areas of rectangles shown in *A*. OS, outer segments; ONL, outer nuclear layer; INL, inner nuclear layer. (*C*) Representative immunostaining of Rho (green) in the central areas of 6-mo-old WT, KI, and KI;*Fatp4*$^{-/-}$ mouse superior retinas. (*D*) Immunoblot analysis of Rho in the retinas of 2- and 4-mo-old WT, KI, and KI;*Fatp4*$^{-/-}$ mice. (*E*) Relative expression levels of Rho in the KI and KI;*Fatp4*$^{-/-}$ retinas were normalized by actin levels and shown as percent of Rho levels in the WT retinas. Asterisks indicate significant differences between KI and KI;*Fatp4*$^{-/-}$ mice (*$P < 0.03$, **$P \leq 0.004$). Error bars show SD ($n = 3$).

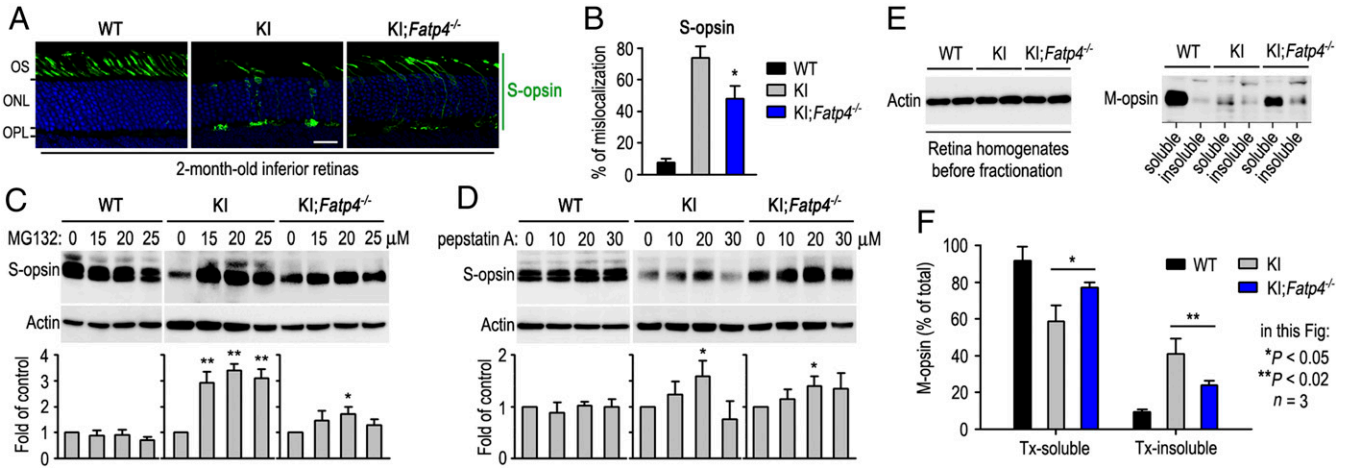

Fig. 4. Improved trafficking, stability, and solubility of cone opsins in KI;*Fatp4*$^{-/-}$ mice. (*A*) S-opsin (green) immunohistochemistry in WT, KI, and KI;*Fatp4*$^{-/-}$ inferior retinas. (Scale bar, 20 μm.) (*B*) Percentage of S-opsin mislocalization estimated by dividing S-opsin immunofluorescence in the OPL by the sum of immunofluorescence in the OPL and OS. Note the decrease in S-opsin mislocalization in KI;*Fatp4*$^{-/-}$ mice. (*C* and *D*) Immunoblot analysis of S-opsin in retinal explants treated with the indicated concentrations of MG132 (*C*) or pepstatin A (*D*). DMSO was used in the MG132 and pepstatin A-null controls. Histograms show relative immunoblot intensities of S-opsin in MG132-treated and pepstatin A-treated retinas versus DMSO-treated controls. (*E*) Representative immunoblot analysis of M-opsin in Triton X-100–soluble and –insoluble retinal fractions separated by ultracentrifugation (*Right*). (*Left*) Immunoblots of actin in the retinal homogenates before ultracentrifugation. (*F*) Percentages of Triton X-100–soluble and –insoluble M-opsin in WT, KI, and KI;*Fatp4*$^{-/-}$ mice are estimated from the immunoblot intensities in *E*.

As a result, the number of S-cones preserved in the inferior retinas of 6-mo-old KI;*Fatp4*$^{+/-}$ and KI;*Fatp4*$^{-/-}$ was ~4.5-fold or 13.5-fold greater than those in age-matched KI mouse inferior retinas (Fig. 5 *J* and *K*). Immunoblot analysis confirmed that S-opsin was almost undetectable in 6-mo-old KI mouse inferior retinas while KI;*Fatp4*$^{-/-}$ mouse inferior retinas still contained a significant amount of S-opsin at the same age (Fig. 5*L*). The results described above indicate that the degrees of S-cone degeneration are negatively correlated with the expression levels of FATP4 in the RPE of the three LCA models at 2, 4, and 6 mo of age.

Inverse Correlation between Visual Function and FATP4 Expression in the LCA Mouse Lines. To test whether FATP4-deficiency improves the visual function, we recorded scotopic and photopic ERG responses in KI and KI;*Fatp4*$^{-/-}$ mice. As shown in Fig. 7 *A*–*D*, photoresponses of both rods and cones in KI;*Fatp4*$^{-/-}$ mice were significantly greater than those in KI mice. To evaluate the function of S- and M-cones separately, we recorded ERG responses with UV and green lights. Amplitudes of S-cone *b*-waves evoked by UV flashes were significantly higher in KI;*Fatp4*$^{+/-}$ and KI;*Fatp4*$^{-/-}$ mice, as compared to KI mice (Fig. 7 *E* and *F*); *b*-wave amplitudes of M-cones in KI;*Fatp4*$^{-/-}$ mice were also greater than those of the KI mouse M-cones (Fig. 7 *G* and *H*).

Discussion

In this study, we have established FATP4 as a therapeutic target by providing evidence that FATP4-deficiency in the RPE increases the synthesis of 11*c*RAL and 9*c*RAL, improving the visual cycle, rod light sensitivity, as well as stability, solubility, and trafficking of cone opsins in mouse models of LCA. We further showed that survival and function of cones are significantly enhanced in KI;*Fatp4*$^{-/-}$ mice, and are negatively correlated with FATP4 expression levels in the RPE of KI, KI;*Fatp4*$^{+/-}$, and KI;*Fatp4*$^{-/-}$ mice. These findings suggest that pharmacological approaches suppressing FATP4 expression have the potential to mitigate cone degeneration and vision loss in patients with RPE65 mutations.

RPE65 uses all-*trans* retinyl fatty acid esters (*at*RE) as its substrate to synthesize 11*c*ROL (2). The fatty acid moiety of *at*RE is crucial for binding with RPE65 and may facilitate substrate access to the catalytic site located inside a hydrophobic pocket of RPE65 (39). In agreement with these studies, our previous experiments showed that FATP4 competes with RPE65 for the *at*RE substrate of RPE65 (28). In addition, our recent study indicates that interaction between FATP4 and RPE65 also contributes to inhibition of the RPE65-catalyzed synthesis of 11*c*ROL (32). These studies suggest that enhancement of all-*trans* to 11-*cis* isomerization catalyzed by R91W RPE65 is the main mechanism for rescuing the visual cycle in the KI mice lacking FATP4. Although the RPE retinal G protein-coupled receptor (RGR) also catalyzes the all-*trans* to 11-*cis* isomerization to make 11*c*RAL (40–42), the following data suggest that FATP4-deficiency promoted the RPE65-catalyzed isomerization rather than the RGR-mediated isomerization: 1) Amplitudes of scotopic ERG *a*-waves in 30- or 45-min dark-adapted KI;*Fatp4*$^{-/-}$ mice were much higher than those in KI mice under the same dark-adaptation conditions (Fig. 2 *A* and *B*), and 2) the amount of 11*c*RAL synthesized during 1-h dark adaptation of KI;*Fatp4*$^{-/-}$ mice was significantly greater than that in KI mice under the same conditions (Fig. 2*C*). These results indicate that FATP4-deficiency promoted 11*c*RAL synthesis in a light-independent mechanism, while RGR-mediated synthesis of 11*c*RAL requires light stimuli (40–42).

Similar to the early cone degeneration phenotypes in dogs and mice with *Rpe65* mutations (34, 43, 44), patients with some RPE65 mutations (including R91W mutation) exhibit a significant loss of cones at very early ages (14, 15, 33, 45). Mislocalization of cone opsins may contribute to the early cone degeneration in the *Rpe65*$^{-/-}$ and KI mice (5, 34). In this study, we observed that FATP4-deficiency in the RPE significantly reduced mislocalization of S-opsin in the KI mice (Fig. 4 *A* and *B*). This mitigation of S-opsin mislocalization is most likely due to an increase in correct folding of S-opsin rather than correcting a trafficking defect of the opsin. Visual chromophores of 11*c*RAL and 9*c*RAL have been shown to function as chaperones for effective folding of mutated opsin (46). These data suggest that 11*c*RAL and 9*c*RAL increased in the KI;*Fatp4*$^{-/-}$ retina promoted the native folding of cone opsins, which in turn improved

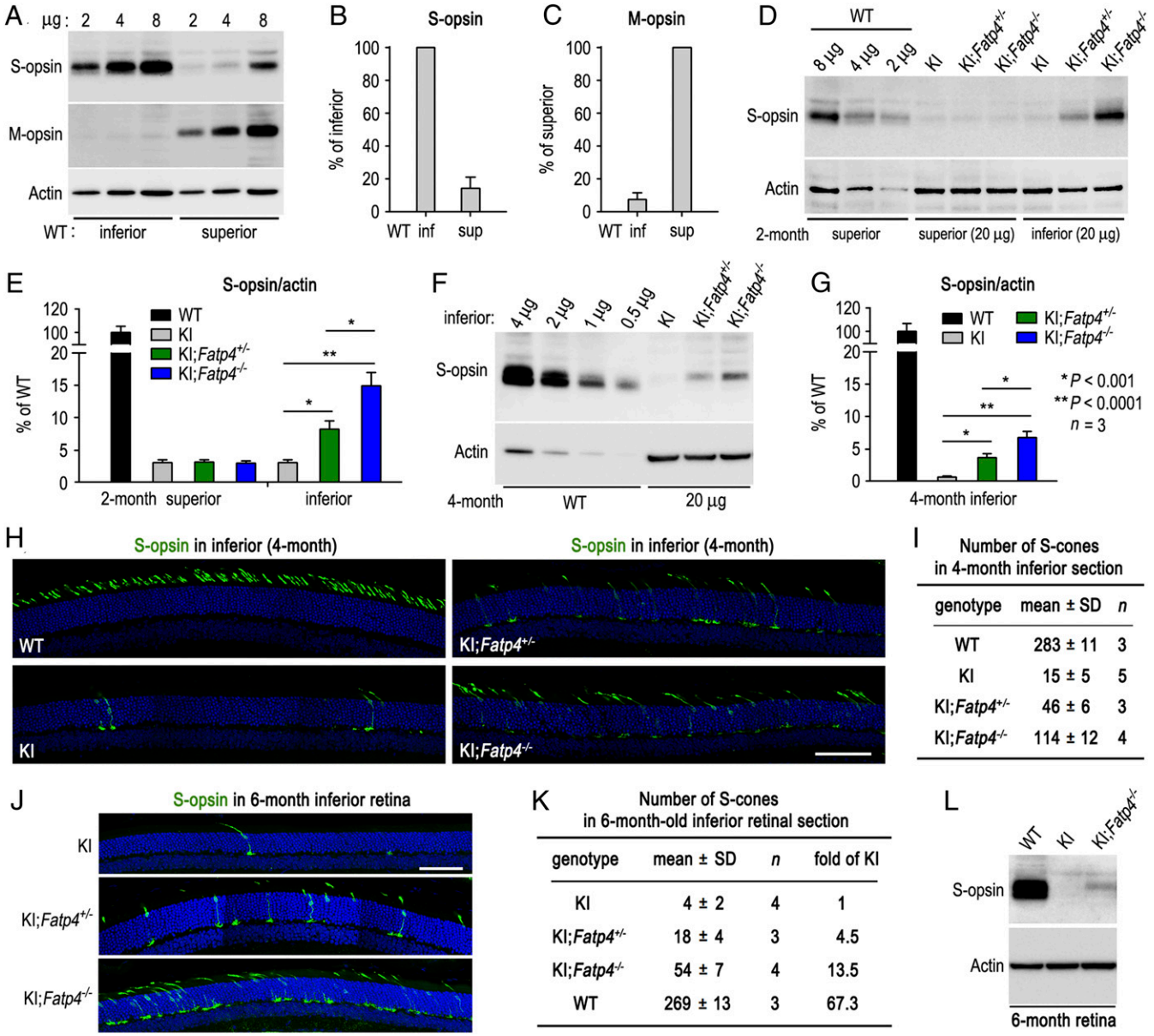

Fig. 5. Inverse correlation between S-cone degeneration and FATP4 expression in KI mouse models. (*A*) Immunoblot analysis of S- and M-opsins in the indicated amounts (μg) of retinal homogenates from inferior or superior halves of WT mouse retinas. (*B* and *C*) Percentages of S-opsin (*B*) and M-opsin (*C*) included in the inferior and superior halves of WT retinas. (*D*) Immunoblot analysis of S-opsin in the inferior and superior halves of 2-mo-old mouse retinas with the indicated genotypes. (*E*) Relative expression levels of S-opsin in the inferior or superior halves of 2-mo-old KI, KI;*Fatp4*$^{+/-}$, and KI;*Fatp4*$^{-/-}$ retinas are shown as percent of S-opsin levels in the inferior or superior halves of WT retinas. (*F*) Immunoblot analysis of S-opsin in the inferior halves of 4-mo-old WT, KI, KI;*Fatp4*$^{+/-}$, and KI;*Fatp4*$^{-/-}$ mouse retinas. (*G*) Relative expression levels of S-opsin in the inferior half of 4-mo-old KI, KI;*Fatp4*$^{+/-}$, and KI;*Fatp4*$^{-/-}$ retinas are shown as percent of S-opsin levels in age-matched WT inferior retinas. (*H*) Immunostaining of S-opsin in the inferior retinas of 4-mo-old WT, KI, KI;*Fatp4*$^{+/-}$, and KI;*Fatp4*$^{-/-}$ mice. (Scale bar, 100 μm.) (*I*) Numbers of S-cones in the inferior retinas of sections taken from the dorsal-ventral midline of 4-mo-old mouse eyes. (*J*) Immunostaining of S-opsin in the inferior retinas of 6-mo-old with the indicated genotypes. (Scale bar, 100 μm.) (*K*) Comparison of S-cone numbers in the inferior retinal sections of 6-mo-old mice. (*L*) Immunoblot analysis of S-opsin in 6-mo-old retinas of WT, KI, and KI;*Fatp4*$^{-/-}$ mice. *$P < 0.001$, **$P < 0.0001$, n = 3.

the normal trafficking and stability of S-opsin in the KI;*Fatp4*$^{-/-}$ cones (Fig. 4 *A*–*D*).

To know whether M-opsin is also misfolded in the KI cones, we analyzed M-opsin solubility in Triton X-100, a nonionic detergent that has been used to distinguish normal and misfolded mutant proteins (47, 48). We observed that most of M-opsin proteins in the WT retina were soluble in the Triton X-100–containing homogenate, whereas only ∼60% of M-opsin proteins in the KI retina were soluble under the same detergent conditions (Fig. 4 *E* and *F*). Importantly, soluble fraction of M-opsin proteins was increased to ∼80% in the KI;*Fatp4*$^{-/-}$ retina, while insoluble M-opsin was markedly reduced in the KI;*Fatp4*$^{-/-}$ retina, as compared to the KI retina (Fig. 4 *E* and *F*). These results support the possibility that increased synthesis of the 11*c*RAL and 9*c*RAL chromophores promoted the normal folding of M-opsin, thereby improving the solubility of M-opsin in the KI;*Fatp4*$^{-/-}$ retina.

Of note, we observed that S-opsin in the KI and KI;*Fatp4*$^{-/-}$ cones underwent degradation via both the proteasomal and the

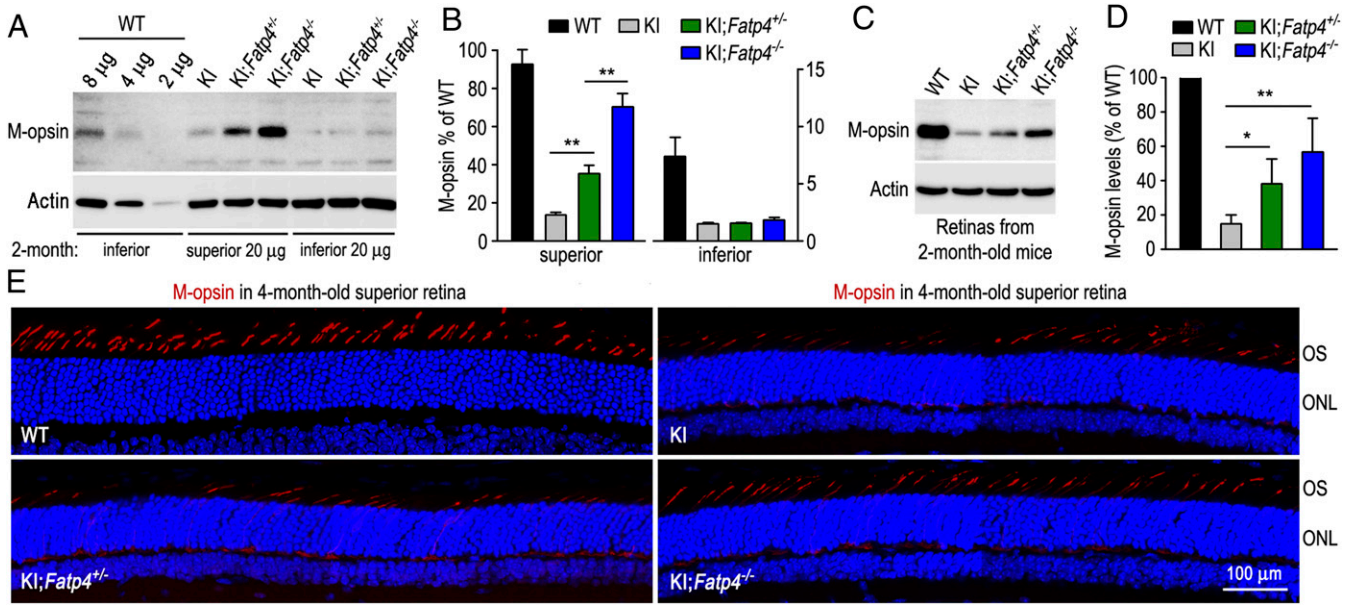

Fig. 6. M-cone preservation is negatively correlated with FATP4 expression in KI mouse lines. (*A*) Immunoblot analysis of M-opsin in the indicated amounts (μg) of retinal homogenates from the inferior or superior halves of WT, KI, KI;*Fatp4*$^{+/-}$, and KI;*Fatp4*$^{-/-}$ mice. (*B*) Expression levels of M-opsin in the superior or inferior halves of 2-mo-old KI, KI;*Fatp4*$^{+/-}$, and KI;*Fatp4*$^{-/-}$ retinas are normalized with actin levels and shown as percent of M-opsin levels in the WT mouse superior or inferior retinas. (*C*) Immunoblot analysis of M-opsin in total retinal homogenates of 2-mo-old WT, KI, KI;*Fatp4*$^{+/-}$, and KI;*Fatp4*$^{-/-}$ mice. (*D*) Histogram showing percentages of normalized M-opsin immunoblot intensities in the mutant retinas relative to the M-opsin intensities in the WT retinas. **P* < 0.01, ***P* < 0.005, n = 3. (*E*) Immunostaining of M-opsin in the superior retinas of 4-mo-old mice with the indicated genotypes.

lysosomal pathways. However, MG132 and pepstatin A displayed significantly different effects on the inhibition of S-opsin degradation in the KI and KI;*Fatp4*$^{-/-}$ retinal explants. As compared to DMSO-treated controls, S-opsin was increased 3-fold or 1.6-fold in the KI and KI;*Fatp4*$^{-/-}$ retinal explants treated with MG132 (Fig. 4*C*), while in the presence of pepstatin A, S-opsin was increased by ∼55% or ∼43% in the KI and KI;*Fatp4*$^{-/-}$ retinal explants, respectively (Fig. 4*D*). These data suggest that the misfolded S-opsin that undergoes the proteasomal degradation in the KI retina is dramatically rescued in the KI;*Fatp4*$^{-/-}$ retina, whereas the misfolded S-opsin that undergoes lysosomal degradation is barely rescued in the KI;*Fatp4*$^{-/-}$ retina. These differences may reflect two different phases of misfolded S-opsin proteins in the mutant cones. In the early phase of misfolding, S-opsin can be refolded by the chromophores that are increased in the KI;*Fatp4*$^{-/-}$ mice; therefore, proteasomal degradation of S-opsin is reduced and MG132 has a significantly smaller effect on increasing S-opsin stability in KI;*Fatp4*$^{-/-}$ retinas compared to KI retinas (Fig. 4*C*). In the late phase of misfolding, S-opsin proteins formed aggregates that undergo lysosomal degradation via the autophagy-mediated autolysosome pathway. The aggregates of misfolded S-opsin may not be refolded by 11*c*RAL and 9*c*RAL; therefore, pepstatin A exhibited a similar effect on S-opsin stability in both KI and KI;*Fatp4*$^{-/-}$ retinas (Fig. 4*D*). These interpretations are in agreement with the following observations: 1) Transmembrane proteins that fail to assume their native structure are subject to ER-associated degradation via the ubiquitin-proteasomal pathway (49); 2) M-opsin undergoes rapid degradation in the proteasomes of *Rpe65*$^{-/-}$ cones (50), whereas ubiquitinated S-opsin accumulates in the *Lrat*$^{-/-}$ cones (51); and 3) autophagy is activated during cone death in animal models of retinal dystrophies (52).

Recent studies showed that a small difference in the intrinsic activities of RPE65 mutants result in a significant difference in photoreceptor survival and function of mice with distinct Rpe65 mutations (25, 34, 37, 53–55). Similar to R91W and F229S substitutions, P25L mutation resulted in a severe decrease in the expression levels of RPE65 and the synthesis rates of 11*c*RAL in mice (37, 54, 55). Reportedly, the isomerase activities of P25L and R91W mutants in the cells are ∼8% or 5% of WT activity, respectively (56, 57). However, in contrast to the R91W and F229S/tvrm148 mice with severe defects in the cone and rod function (34, 37, 53, 54), the P25L mice exhibited relatively mild retinal degeneration and almost normal visual function in both scotopic and photopic ERG recordings (55). In addition, a partial rescue of the R91W mutant with a chemical chaperone (PBA) improved 11*c*RAL synthesis, cone survival, and visual function in KI mice (25).

Compared to the PBA treatment that elevated 11*c*RAL by 96% in the KI mice (25), FATP4-deficiency exhibited a much higher effect on increasing 11*c*RAL synthesis in the KI mice. In the KI;*Fatp4*$^{-/-}$ mice, 11*c*RAL was increased 2.8-fold as compared to KI mice. FATP4-deficiency also promoted the synthesis of 9*c*RAL in the KI mice. Since 9*c*RAL is increased in *Rpe65*$^{-/-}$ mice too (36), 9*c*RAL may be increased via a RPE65-independent pathway in the KI;*Fatp4*$^{-/-}$ mice. Nevertheless, due to the strong rescue of 11*c*RAL and 9*c*RAL synthesis, survival and function of cones dramatically improved in the KI;*Fatp4*$^{-/-}$ mice. Reportedly, mouse lacks the macula pigments (58, 59) and, therefore, the preservation of cones in the KI;*Fatp4*$^{-/-}$ mice may be not related to the *meso*-zeaxanthin synthesis catalyzed by RPE65. Importantly, we found that partial reduction of FATP4 in the RPE significantly improved survival and function of S- and M-cones in KI;*Fatp4*$^{+/-}$ mice (Figs. 5–7). These findings suggest that pharmacological suppression of FATP4 expression has the strong potential to alleviate cone degeneration and color vision loss in patients with RPE65 mutations.

Ezetimibe is an inhibitor of Niemann-Pick C1-like 1 cholesterol influx transporter and a US Food and Drug Administration-approved medication used as an add-on to dietary measures to lower plasma cholesterol. In animal studies, Ezetimibe markedly reduced expression of FATP4 in intestinal cells (60, 61), suggesting that Ezetimibe may be a safe and low-cost

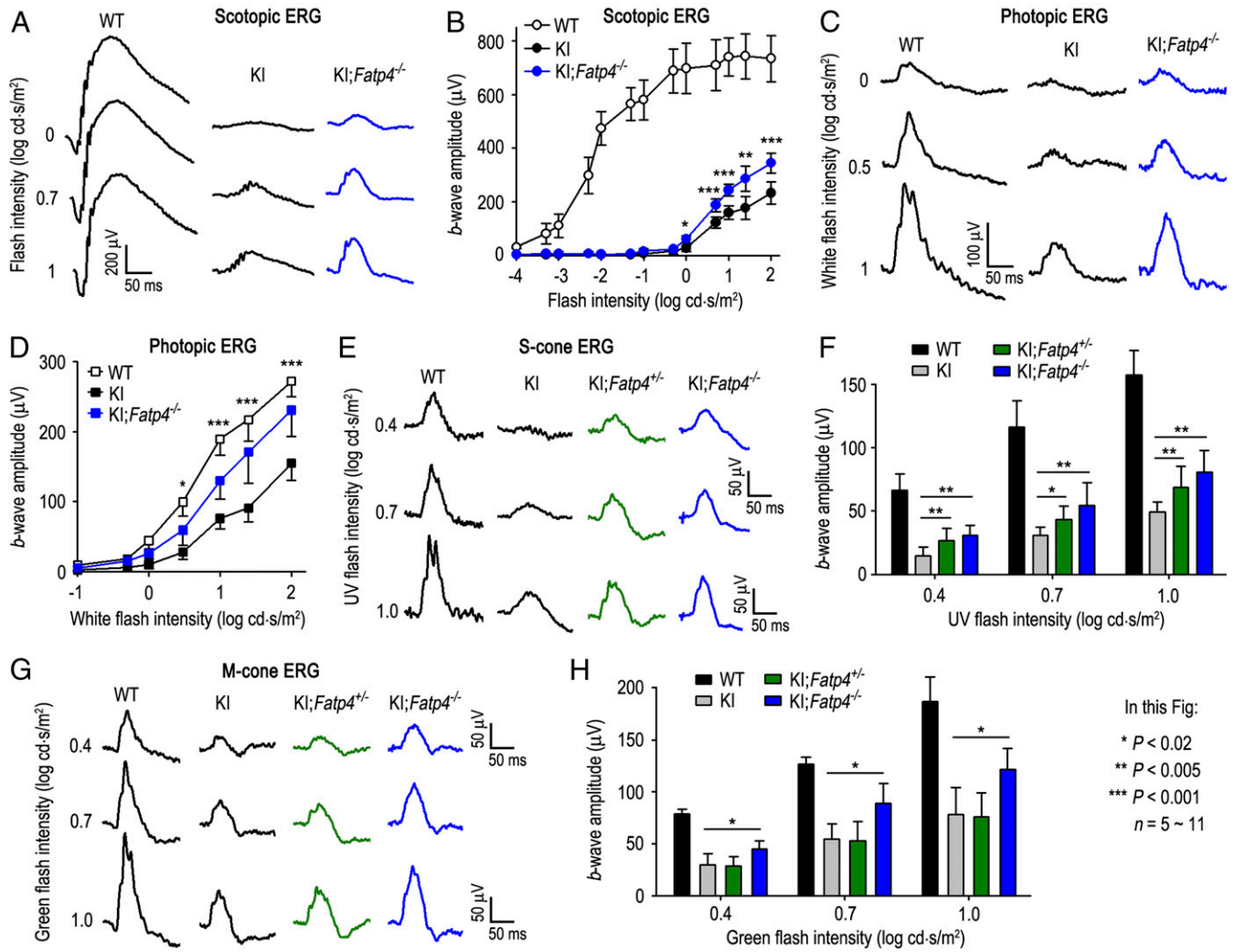

Fig. 7. Inverse correlation between FATP4 expression and visual function of rods and cones in KI mouse models. (*A*) Representative scotopic ERG responses of dark-adapted 6-wk-old WT, KI, and KI;*Fatp4*$^{-/-}$ mice to the indicated flashes (0 ~ 1 log cd·s/m^2). (*B*) Amplitudes of scotopic ERG *b*-waves elicited with the indicated flashes in WT, KI, and KI;*Fatp4*$^{-/-}$ mice. (*C*) Photopic ERG responses of 3-mo-old WT, KI, and KI;*Fatp4*$^{-/-}$ mice to the indicated flashes of white light under a rod-saturating background light. (*D*) Amplitudes of photopic ERG *b*-waves evoked with the indicated light flashes in WT, KI, and KI;*Fatp4*$^{-/-}$ mice. Asterisks indicate significant differences between KI and KI;*Fatp4*$^{-/-}$ mice. (*E*) Representative ERG responses of S-cones in 3-mo-old WT, KI, KI;*Fatp4*$^{+/-}$, and KI;*Fatp4*$^{-/-}$ mice to 360-nm UV light flashes under a rod-saturating background light. (*F*) Amplitudes of S-cone ERG *b*-waves evoked with the indicated intensities of UV light flashes in WT, KI, KI;*Fatp4*$^{+/-}$, and KI;*Fatp4*$^{-/-}$ mice. (*G*) Representative ERG responses of M-cones in 3-mo-old WT and the indicated mutant mice to the flashes of 530-nm green light. (*H*) Amplitudes of M-cone ERG *b*-waves evoked with the indicated intensities of 530-nm light flashes. Asterisks indicate significant differences between KI and KI;*Fatp4*$^{-/-}$ mice.

therapeutic candidate for alleviating retinal degeneration and vision loss in patients with RPE65 mutations. Combination application of Ezetimibe, PBA, and AAV-RPE65 may be an effective intervention for long-term preservation of vision in the patients. To expand the therapeutic application spectrum of our findings, it is important to test whether FATP4-deficiency and Ezetimibe treatment are effective at mitigating the progressive death of photoreceptors in animal models with RPE65-null or other missense mutations.

Materials and Methods

Animals. The *Fatp4*$^{-/-}$;*Ivl-Fatp4*$^{tg/+}$ (shown as *Fatp4*$^{-/-}$ in this study) and R91W KI mice have been described previously (25, 28, 37, 62). Both of these mutant mouse lines have been back-crossed with WT 129S2/Sv strain to generate *Fatp4*$^{-/-}$ and KI mice homozygous for the Leu450 allele of the *Rpe65* gene. We crossed these new KI and new *Fatp4*$^{-/-}$ mice, then intercrossed the heterozygous offspring to yield KI;*Fatp4*$^{-/-}$ and KI;*Fatp4*$^{+/-}$ mice. All animal experiments were performed in accordance with the Association for Research of Vision and Ophthalmology statement for the use of animals in ophthalmic and vision research and the protocols approved by the Institutional Animal Care and Use Committee for Louisiana State University Health Sciences Center.

Immunoblot Analysis. Protein samples were separated by SDS/PAGE and transferred to an Immobilon-P membrane. The membrane was incubated in blocking buffer, primary antibody, and horseradish peroxidase-conjugated anti-rabbit or mouse IgG secondary antibody. Antibodies against RPE65 (63), LRAT (64, 65), FATP4 (66), β-actin, rhodopsin, M-opsin (Millipore Sigma), S-opsin (Santa Cruz Biotechnology) were used as the primary antibodies. Immunoblots were visualized with the ECL Prime Western blotting detection reagent and ImageQuant LAS 4000 (48). Signal intensity of each band was quantified using ImageQuant TL software.

Retinoid Analysis. All tissue manipulations and retinoid analysis were done under dim red light. Retinoids in mouse ocular tissues homogenized with 20 mM Hepes buffer containing 150 mM hydroxylamine were extracted with hexane and analyzed by normal phase HPLCy, as described previously (67). In

brief, retinoids in hexane extractions were evaporated, dissolved in 100 μL of hexane, and separated on a silica column by elution of mobile phase on an Agilent 1100 HPLC system. Spectral data were acquired for all eluted peaks. Quantitation was performed by comparison of peak areas to calibration curves established with authentic retinoid standards. For analysis of the visual cycle rates, dark-adapted mice were exposed to 800 lx light for 5 min, then transferred to darkness. At different times (30 ~ 120 min), eyeballs were enucleated, and retinoids were extracted for HPLC analysis.

Immunohistochemistry. Mouse retinal cryosections prepared from the dorsal-ventral midline of mouse eyes were immunostained as described previously (68). Briefly, mouse eyeballs were fixed with 4% paraformaldehyde in 0.1 M phosphate buffer. After removing cornea and lens, eyecups were immersed in 15% sucrose in PB for 2 h and in 30% sucrose in phosphate buffer overnight at 4 °C, embedded in the OCT medium. Sections cut on a cryostat were immunostained with the primary antibodies and secondary antibodies. Nuclei were counterstained with DAPI. Images were captured with a Zeiss LSM710 Meta confocal microscope. Large images containing 3 × 1 (Fig. 5) or 2 × 1 (Fig. 6) composite images are recorded directly in the Tile Scan mode. Numbers of cone cells were counted using ImageJ software.

Quantification of S-Opsin Mislocalization. Immunostaining of S-opsin was performed on retinal cryosections of 2-mo-old mice, as described above. Fluorescence intensities in the OS and the retinal outer plexiform layer (OPL) were measured using an Olympus BX61VS microscope. We determined the fraction of mislocalized S-opsin according to the following formula. Mislocalization = [OPL fluorescence/(OS fluorescence + OPL fluorescence)] × 100%.

Protease Inhibitor Assay. Eyes were enucleated from euthanized 4-wk-old mice, and the corneas and lenses were removed. The neural retinas dissected from the eyecups were maintained in the DMEM-F12 medium (Thermo Fisher Scientific) supplemented with 10% fetal bovine serum and antibiotics in a 5% CO_2 incubator at 37 °C. After incubating for 5 h in the presence of a series of increasing concentrations of MG132 (0 ~ 25 μM) or pepstatin A (0 ~ 30 μM), the retinas were subjected to immunoblot analysis.

Quantification of Soluble and Insoluble Opsins. Retinas were homogenized in ice-cold PBS containing 0.4% Triton X-100 and EDTA-free protease inhibitor mixtures. The homogenates containing 100 μg proteins were separated into supernatant and pellet by centrifugation at 100,000 × *g* for 20 min at 4 °C. The pellet was washed twice with ice-cold PBS and resuspended in 20 μL lysis buffer (PBS, 0.1% SDS and 0.4% Triton X-100). Ten microliters of the resuspended pellet and the supernatant containing soluble proteins were subjected to immunoblot analysis. Percent of soluble and insoluble opsin was calculated using the following formula: Soluble or insoluble opsin % = [immunoblot intensity in soluble (or insoluble) fraction/sum of immunoblot intensities in soluble and insoluble fractions] × 100%.

ERG. Dark-adapted mice were anesthetized with an intraperitoneal injection of Ketamine-Xylazine mixture and the pupils were dilated with 1% tropicamide. ERG was recorded from the corneal surface using a silver–silver chloride wire electrode referenced to a subcutaneous electrode in the mouth. A needle electrode in the tail served as the ground. A drop of 2.5% methylcellulose was placed on the cornea. ERG recordings were performed in a Ganzfield dome (Espion e2, Diagnosys) with various intensities of single flash stimuli (–4 log cd·s/m^2 ~ 2.4 log cd·s/m^2). For photopic ERGs, animals were light-adapted for 10 min by exposing to 32 cd/m^2 light, and ERG responses were obtained with white flashes on the rod-saturating background (32 cd/m^2). For recording S- and M-cone ERG responses, animals were light-adapted for 10 min by exposing to 40 cd/m^2 white light. S-cone ERGs were obtained with xenon flashes equipped with a Hoya U-360 filter on the 40 cd/m^2 background, and M-cone ERGs were elicited with stimuli of 530-nm light. Intensity-response amplitude data were displayed on log-linear coordinates using the SigmaPlot 11 software.

Statistical Analysis. All statistical analyses were performed using the SigmaPlot v11 (Systat Software). Data were expressed as the mean ± SD of three or more independent experiments. Significant differences between distinct genotypes of mice were determined by single comparisons with an unpaired two-tailed Student's *t* test. The significance threshold was set at 0.05 for all statistical tests.

Data Availability. All study data are included in the article and supporting information.

ACKNOWLEDGMENTS. We thank Dr. Jeffery H. Miner for the *Fatp4*$^{-/-}$;*Ivl-Fatp4*$^{tg/+}$ mice and Dr. Christian Grimm for the R91W knockin mice. This work was supported by NIH Grants EY021208, EY028572, and EY028255 (to M.J.), and GM103340 and EY005121 (to N.G.B.); the Louisiana State University School of Medicine Research Enhancement Fund (M.J.); and Eye, Ear, Nose, Throat Foundation of New Orleans (W.C.G., N.G.B.).

1. T. M. Redmond *et al.*, Rpe65 is necessary for production of 11-*cis*-vitamin A in the retinal visual cycle. *Nat. Genet.* **20**, 344–351 (1998).
2. M. Jin, S. Li, W. N. Moghrabi, H. Sun, G. H. Travis, Rpe65 is the retinoid isomerase in bovine retinal pigment epithelium. *Cell* **122**, 449–459 (2005).
3. G. Moiseyev, Y. Chen, Y. Takahashi, B. X. Wu, J. X. Ma, RPE65 is the isomerohydrolase in the retinoid visual cycle. *Proc. Natl. Acad. Sci. U.S.A.* **102**, 12413–12418 (2005).
4. T. M. Redmond *et al.*, Mutation of key residues of RPE65 abolishes its enzymatic role as isomerohydrolase in the visual cycle. *Proc. Natl. Acad. Sci. U.S.A.* **102**, 13658–13663 (2005).
5. B. Rohrer *et al.*, Cone opsin mislocalization in Rpe65-/- mice: A defect that can be corrected by 11-cis retinal. *Invest. Ophthalmol. Vis. Sci.* **46**, 3876–3882 (2005).
6. H. Zhang *et al.*, Trafficking of membrane-associated proteins to cone photoreceptor outer segments requires the chromophore 11-*cis*-retinal. *J. Neurosci.* **28**, 4008–4014 (2008).
7. R. Shyam, A. Gorusupudi, K. Nelson, M. P. Horvath, P. S. Bernstein, RPE65 has an additional function as the lutein to *meso*-zeaxanthin isomerase in the vertebrate eye. *Proc. Natl. Acad. Sci. U.S.A.* **114**, 10882–10887 (2017).
8. P. S. Bernstein *et al.*, Lutein, zeaxanthin, and meso-zeaxanthin: The basic and clinical science underlying carotenoid-based nutritional interventions against ocular disease. *Prog. Retin. Eye Res.* **50**, 34–66 (2016).
9. A. Wenzel, C. E. Reme, T. P. Williams, F. Hafezi, C. Grimm, The Rpe65 Leu450Met variation increases retinal resistance against light-induced degeneration by slowing rhodopsin regeneration. *J. Neurosci.* **21**, 53–58 (2001).
10. S. Li *et al.*, Ciliary neurotrophic factor (CNTF) protects retinal cone and rod photoreceptors by suppressing excessive formation of the visual pigments. *J. Biol. Chem.* **293**, 15256–15268 (2018).
11. S. R. Kim *et al.*, Rpe65 Leu450Met variant is associated with reduced levels of the retinal pigment epithelium lipofuscin fluorophores A2E and iso-A2E. *Proc. Natl. Acad. Sci. U.S.A.* **101**, 11668–11672 (2004).
12. J. Weng *et al.*, Insights into the function of Rim protein in photoreceptors and etiology of Stargardt's disease from the phenotype in abcr knockout mice. *Cell* **98**, 13–23 (1999).
13. S. Schmitz-Valckenberg *et al.*; Fundus Autofluorescence in Age-Related Macular Degeneration Study Group, Correlation between the area of increased autofluorescence surrounding geographic atrophy and disease progression in patients with AMD. *Invest. Ophthalmol. Vis. Sci.* **47**, 2648–2654 (2006).
14. S. G. Jacobson *et al.*, Identifying photoreceptors in blind eyes caused by RPE65 mutations: Prerequisite for human gene therapy success. *Proc. Natl. Acad. Sci. U.S.A.* **102**, 6177–6182 (2005).
15. S. G. Jacobson *et al.*, Defining the residual vision in leber congenital amaurosis caused by RPE65 mutations. *Invest. Ophthalmol. Vis. Sci.* **50**, 2368–2375 (2009).
16. S. G. Jacobson *et al.*, Human cone photoreceptor dependence on RPE65 isomerase. *Proc. Natl. Acad. Sci. U.S.A.* **104**, 15123–15128 (2007).
17. J. W. Bainbridge *et al.*, Effect of gene therapy on visual function in Leber's congenital amaurosis. *N. Engl. J. Med.* **358**, 2231–2239 (2008).
18. A. V. Cideciyan *et al.*, Human gene therapy for RPE65 isomerase deficiency activates the retinoid cycle of vision but with slow rod kinetics. *Proc. Natl. Acad. Sci. U.S.A.* **105**, 15112–15117 (2008).
19. W. W. Hauswirth *et al.*, Treatment of leber congenital amaurosis due to RPE65 mutations by ocular subretinal injection of adeno-associated virus gene vector: Short-term results of a phase I trial. *Hum. Gene Ther.* **19**, 979–990 (2008).
20. A. M. Maguire *et al.*, Safety and efficacy of gene transfer for Leber's congenital amaurosis. *N. Engl. J. Med.* **358**, 2240–2248 (2008).
21. A. V. Cideciyan *et al.*, Human retinal gene therapy for Leber congenital amaurosis shows advancing retinal degeneration despite enduring visual improvement. *Proc. Natl. Acad. Sci. U.S.A.* **110**, E517–E525 (2013).
22. S. G. Jacobson *et al.*, Improvement and decline in vision with gene therapy in childhood blindness. *N. Engl. J. Med.* **372**, 1920–1926 (2015).
23. J. W. Bainbridge *et al.*, Long-term effect of gene therapy on Leber's congenital amaurosis. *N. Engl. J. Med.* **372**, 1887–1897 (2015).
24. W. Xiong *et al.*, AAV *cis*-regulatory sequences are correlated with ocular toxicity. *Proc. Natl. Acad. Sci. U.S.A.* **116**, 5785–5794 (2019).
25. S. Li, M. Samardzija, Z. Yang, C. Grimm, M. Jin, Pharmacological amelioration of cone survival and vision in a mouse model for Leber congenital amaurosis. *J. Neurosci.* **36**, 5808–5819 (2016).
26. S. Li *et al.*, Rescue of enzymatic function for disease-associated RPE65 proteins containing various missense mutations in non-active sites. *J. Biol. Chem.* **289**, 18943–18956 (2014).
27. S. Li *et al.*, Temperature-sensitive retinoid isomerase activity of RPE65 mutants associated with Leber congenital amaurosis. *J. Biochem.* **158**, 115–125 (2015).

28. S. Li *et al*., Fatty acid transport protein 4 (FATP4) prevents light-induced degeneration of cone and rod photoreceptors by inhibiting RPE65 isomerase. *J. Neurosci.* **33**, 3178–3189 (2013).
29. K. Milger *et al*., Cellular uptake of fatty acids driven by the ER-localized acyl-CoA synthetase FATP4. *J. Cell Sci.* **119**, 4678–4688 (2006).
30. A. M. Hall, B. M. Wiczer, T. Herrmann, W. Stremmel, D. A. Bernlohr, Enzymatic properties of purified murine fatty acid transport protein 4 and analysis of acyl-CoA synthetase activities in tissues from FATP4 null mice. *J. Biol. Chem.* **280**, 11948–11954 (2005).
31. Z. Jia, C. L. Moulson, Z. Pei, J. H. Miner, P. A. Watkins, Fatty acid transport protein 4 is the principal very long chain fatty acyl-CoA synthetase in skin fibroblasts. *J. Biol. Chem.* **282**, 20573–20583 (2007).
32. S. Li, J. F. Green, M. Jin, Impacts of deletion and ichthyosis prematurity syndrome-associated mutations in fatty acid transport protein 4 on the function of RPE65. *FEBS Lett.* **594**, 540–552 (2020).
33. S. G. Jacobson *et al*., Photoreceptor layer topography in children with Leber congenital amaurosis caused by RPE65 mutations. *Invest. Ophthalmol. Vis. Sci.* **49**, 4573–4577 (2008).
34. M. Samardzija *et al*., In conditions of limited chromophore supply rods entrap 11-cis-retinal leading to loss of cone function and cell death. *Hum. Mol. Genet.* **18**, 1266–1275 (2009).
35. M. Lee, S. Li, K. Sato, M. Jin, Interphotoreceptor retinoid-binding protein mitigates cellular oxidative stress and mitochondrial dysfunction induced by all-trans-retinal. *Invest. Ophthalmol. Vis. Sci.* **57**, 1553–1562 (2016).
36. J. Fan, B. Rohrer, G. Moiseyev, J. X. Ma, R. K. Crouch, Isorhodopsin rather than rhodopsin mediates rod function in RPE65 knock-out mice. *Proc. Natl. Acad. Sci. U.S.A.* **100**, 13662–13667 (2003).
37. M. Samardzija *et al*., R91W mutation in Rpe65 leads to milder early-onset retinal dystrophy due to the generation of low levels of 11-*cis*-retinal. *Hum. Mol. Genet.* **17**, 281–292 (2008).
38. A. Szél *et al*., Unique topographic separation of two spectral classes of cones in the mouse retina. *J. Comp. Neurol.* **325**, 327–342 (1992).
39. P. D. Kiser, M. Golczak, D. T. Lodowski, M. R. Chance, K. Palczewski, Crystal structure of native RPE65, the retinoid isomerase of the visual cycle. *Proc. Natl. Acad. Sci. U.S.A.* **106**, 17325–17330 (2009).
40. P. Chen *et al*., A photic visual cycle of rhodopsin regeneration is dependent on Rgr. *Nat. Genet.* **28**, 256–260 (2001).
41. A. Morshedian *et al*., Light-driven regeneration of cone visual pigments through a mechanism involving RGR opsin in Muller glial cells. *Neuron* **102**, 1172–1183.e5 (2019).
42. J. Zhang *et al*., Photic generation of 11-*cis*-retinal in bovine retinal pigment epithelium. *J. Biol. Chem.* **294**, 19137–19154 (2019).
43. G. M. Acland *et al*., Long-term restoration of rod and cone vision by single dose rAAV-mediated gene transfer to the retina in a canine model of childhood blindness. *Mol. Ther.* **12**, 1072–1082 (2005).
44. S. L. Znoiko *et al*., Downregulation of cone-specific gene expression and degeneration of cone photoreceptors in the Rpe65-/- mouse at early ages. *Invest. Ophthalmol. Vis. Sci.* **46**, 1473–1479 (2005).
45. C. Jakobsson, I. S. Othman, F. L. Munier, D. F. Schorderet, H. Abouzeid, Cone-rod dystrophy caused by a novel homozygous RPE65 mutation in Leber congenital amaurosis. *Klin. Monatsbl. Augenheilkd.* **231**, 405–410 (2014).
46. R. S. Saliba, P. M. Munro, P. J. Luthert, M. E. Cheetham, The cellular fate of mutant rhodopsin: Quality control, degradation and aggresome formation. *J. Cell Sci.* **115**, 2907–2918 (2002).
47. Z. Zhou, D. Vollrath, A cellular assay distinguishes normal and mutant TIGR/myocilin protein. *Hum. Mol. Genet.* **8**, 2221–2228 (1999).
48. S. Li *et al*., Secretory defect and cytotoxicity: The potential disease mechanisms for the retinitis pigmentosa (RP)-associated interphotoreceptor retinoid-binding protein (IRBP). *J. Biol. Chem.* **288**, 11395–11406 (2013).
49. J. H. Lin *et al*., IRE1 signaling affects cell fate during the unfolded protein response. *Science* **318**, 944–949 (2007).
50. K. Sato, T. Ozaki, S. Ishiguro, M. Nakazawa, M-opsin protein degradation is inhibited by MG-132 in Rpe65$^{-/-}$ retinal explant culture. *Mol. Vis.* **18**, 1516–1525 (2012).
51. T. Zhang, N. Zhang, W. Baehr, Y. Fu, Cone opsin determines the time course of cone photoreceptor degeneration in Leber congenital amaurosis. *Proc. Natl. Acad. Sci. U.S.A.* **108**, 8879–8884 (2011).
52. C. Punzo, K. Kornacker, C. L. Cepko, Stimulation of the insulin/mTOR pathway delays cone death in a mouse model of retinitis pigmentosa. *Nat. Neurosci.* **12**, 44–52 (2009).
53. J. Won *et al*., Mouse model resources for vision research. *J. Ophthalmol.* **2011**, 391384 (2011).
54. C. B. Wright *et al*., Complementation test of Rpe65 knockout and tvrm148. *Invest. Ophthalmol. Vis. Sci.* **54**, 5111–5122 (2013).
55. Y. Li *et al*., Mouse model of human RPE65 P25L hypomorph resembles wild type under normal light rearing but is fully resistant to acute light damage. *Hum. Mol. Genet.* **24**, 4417–4428 (2015).
56. B. Lorenz *et al*., A comprehensive clinical and biochemical functional study of a novel RPE65 hypomorphic mutation. *Invest. Ophthalmol. Vis. Sci.* **49**, 5235–5242 (2008).
57. A. R. Philp *et al*., Predicting the pathogenicity of RPE65 mutations. *Hum. Mutat.* **30**, 1183–1188 (2009).
58. B. Li *et al*., Inactivity of human β,β-carotene-9′,10′-dioxygenase (BCO2) underlies retinal accumulation of the human macular carotenoid pigment. *Proc. Natl. Acad. Sci. U.S.A.* **111**, 10173–10178 (2014).
59. B. Li *et al*., Retinal accumulation of zeaxanthin, lutein, and β-carotene in mice deficient in carotenoid cleavage enzymes. *Exp. Eye Res.* **159**, 123–131 (2017).
60. E. D. Labonté *et al*., Reduced absorption of saturated fatty acids and resistance to diet-induced obesity and diabetes by ezetimibe-treated and Npc1l1-/- mice. *Am. J. Physiol. Gastrointest. Liver Physiol.* **295**, G776–G783 (2008).
61. M. Naples *et al*., Ezetimibe ameliorates intestinal chylomicron overproduction and improves glucose tolerance in a diet-induced hamster model of insulin resistance. *Am. J. Physiol. Gastrointest. Liver Physiol.* **302**, G1043–G1052 (2012).
62. C. L. Moulson *et al*., Keratinocyte-specific expression of fatty acid transport protein 4 rescues the wrinkle-free phenotype in Slc27a4/Fatp4 mutant mice. *J. Biol. Chem.* **282**, 15912–15920 (2007).
63. M. Jin, Q. Yuan, S. Li, G. H. Travis, Role of LRAT on the retinoid isomerase activity and membrane association of Rpe65. *J. Biol. Chem.* **282**, 20915–20924 (2007).
64. M. L. Batten *et al*., Lecithin-retinol acyltransferase is essential for accumulation of all-trans-retinyl esters in the eye and in the liver. *J. Biol. Chem.* **279**, 10422–10432 (2004).
65. M. Golczak, V. Kuksa, T. Maeda, A. R. Moise, K. Palczewski, Positively charged retinoids are potent and selective inhibitors of the trans-*cis* isomerization in the retinoid (visual) cycle. *Proc. Natl. Acad. Sci. U.S.A.* **102**, 8162–8167 (2005).
66. E. P. Newberry *et al*., Decreased hepatic triglyceride accumulation and altered fatty acid uptake in mice with deletion of the liver fatty acid-binding protein gene. *J. Biol. Chem.* **278**, 51664–51672 (2003).
67. M. Jin *et al*., The role of interphotoreceptor retinoid-binding protein on the translocation of visual retinoids and function of cone photoreceptors. *J. Neurosci.* **29**, 1486–1495 (2009).
68. K. Sato *et al*., Receptor interacting protein kinase-mediated necrosis contributes to cone and rod photoreceptor degeneration in the retina lacking interphotoreceptor retinoid-binding protein. *J. Neurosci.* **33**, 17458–17468 (2013).